

CHARACTERIZATION OF A HIGH CURRENT INDUCTION ACCELERATOR ELECTRON BEAM VIA OPTICAL TRANSITION RADIATION FROM DIELECTRIC FOILS*

V. Tang[#], C. Brown and T. Houck, LLNL, Livermore, CA 94551, U.S.A.

Abstract

Traditionally, thin metal foils are employed for optical transition radiation (OTR) beam diagnostics but the possibility of shorting accelerator insulating surfaces and modifying accelerating fields are concerns. The successful utilization of dielectric foils in place of metal ones could alleviate these issues but necessitates more understanding of the OTR data for inferring desired beam parameters because of the dielectric's finite permittivity. Additionally, the temperature dependence of the relevant foil parameters due to beam heating should be accounted for. Here, we present and discuss sample synthetic diagnostic results of Kapton OTR spot-size measurements from the Flash X-Ray (FXR) accelerator which studies these and sightline effects. These simulations show that in some cases, the observed spot-sizes and radii are noticeably larger than the beam radii.

INTRODUCTION

The successful utilization of dielectric foils for OTR based divergence and spot size measurements in high current accelerators would alleviate some of the practical concerns associated with employing metal foils and allow greater design flexibility. The concerns with metal foils include the possibility of plating or shorting insulator surfaces, and modifying the accelerating field structure. However, because of the finite permittivity of the dielectric foils, using dielectric foils for OTR requires more modeling of the data in order to extract useful information. Additionally, the foil could have a non-uniform permittivity profile due to a non-uniform temperature profile. In this work, we present synthetic diagnostic results of OTR spot-size measurements from the FXR induction accelerator [1] which is capable of producing ~3 kA of 17.5 MeV electrons in a ~70 ns pulse. Instantaneous heating of the foil during a pulse, and shot-to-shot temperature buildup of the foil are both examined. The synthetic diagnostic results show that the observed spot-size and radii can be noticeably larger than the real beam radii, due to both the anisotropic nature of OTR and the studied temperature effects. These results and models are considered in order to interpret properly some of the data from the dielectric foil OTR diagnostic [2-4] on FXR.

MODEL DETAILS

In this section, we review the FXR OTR diagnostic

* Work supported by U.S. DOE Contract W-7405-Eng-48

[#]tang23@llnl.gov

setup and the details of the synthetic diagnostic. A specific case of an FXR beam with a non-divergent Gaussian current profile hitting a 0.127 mm thick Kapton foil placed 45 degrees to the beam is examined.

Diagnostic Setup and OTR emission

The portion of the FXR OTR diagnostic considered here primarily consists of a 60 mm f/2.8D Nikon collection lens ~25 cm away from a rotatable ~11 cm diameter OTR foil. Kapton or quartz dielectric foils can be employed. The diagnostic can be setup for either angular or spot-size (spatial) imaging. The signal is coupled via optical fibers to a fast CCD camera typically operated with gate widths of ~2 ns. Usually, the diagnostic is setup to view the specular reflection at 45 degrees. The setup is schematically illustrated in Figure 1. The synthetic diagnostic discussed here aims to simulate the detected OTR emission along a thin vertical strip at the center of a Kapton foil.

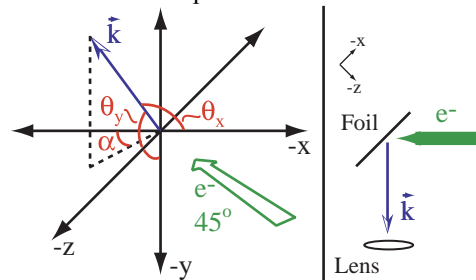


Figure 1: Coordinate and Experimental setup. The diagnosed beam traverses at 45 degrees a dielectric foil in the x-y plane. The OTR emission from each point on the foil (i.e. origin on the left) is represented by the vector k and varies depending on angles θ_y and α . A unit normal from the lens' center lies on the x-z plane. Emission from the center of the foil detected using the lowest f-number of the lens comes from a solid angle covering $\alpha=45\pm 2.5$ deg and $\theta_y=90\pm 2.5$ deg.

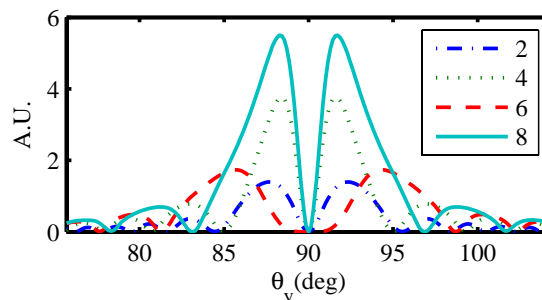


Figure 2: OTR emission at 2 eV for a 0.1265 mm thick dielectric foil with $\epsilon=2$ to 8 at $\alpha=45$ degrees.

The relevant OTR equations for dielectric foils with arbitrary geometry were noted by Ter-Mikaelian [5]. The permittivity dependence of the OTR emission, assuming no beam divergence, can be seen in Figure 2. The emission is a sum of both perpendicular and parallel polarization. Integrating the emission over the relevant photon energies of 1.7 to 6.2 eV with the FXR camera efficiencies averages out the interferometer effects in Figure 2 and results in the smooth profiles shown in Figure 3. The peak of the emission profiles is $\sim 1/\gamma$, similar to OTR from metallic foils. The permittivity dependence is roughly proportional to $-\epsilon^2 + 16\epsilon - 15$ at the $1/\gamma$ peak for $\epsilon=1$ to 8 but varies moderately with θ_v and α .

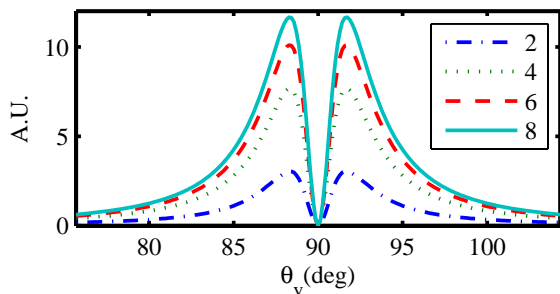


Figure 3: OTR emission from Figure 2 integrated from 1.7 to 6.2 eV with camera efficiencies.

Temperature and Permittivity Profile

The temperature of the Kapton foil during a shot is modeled assuming a constant heat capacity of 1.09 J/gm-K [6], ρ of 1.42 gm/cc [6], and a foil heating of $\sim 3.4 \times 10^{13}$ J/cm foil thickness per electron [4]. For a Gaussian beam with r_{rms} of 0.5 cm hitting a foil initially at room temperature, this results in a temperature profile mid-pulse shown in Figure 4. This profile can be used to determine any temperature dependent permittivity OTR effects and also to prevent melting of the foil.

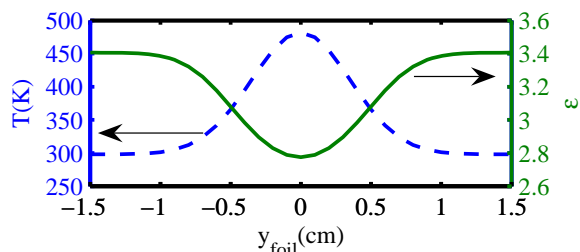


Figure 4: Mid-shot Kapton foil temperature and sample permittivity profiles along a center vertical strip for a Gaussian current profile with an r_{rms} of 0.5 cm.

With the temperature profile determined, the required permittivity can be estimated. For Kapton, the room temperature permittivity is ~ 3.4 in the relevant photon energies [7]. The moderate imaginary component is ignored for simplicity. A simple Debye model [8] is used for the temperature dependence due to a lack of experimental data and results in the permittivity profile shown in Figure 4. The Debye model is strictly not applicable at the optical frequencies of concern, but useful nevertheless for illustrative purposes here. More accurate

permittivity models or data at optical frequencies as a function of temperature are needed and are part of ongoing work. The Debye model gives:

$$\frac{\epsilon - 1}{\epsilon + 2} = \beta \left(\alpha(\omega) + \frac{\mu^2}{3k_b T} \right)$$

Where β is 8.4×10^{37} J/C²m², $\alpha(\omega)$ is $\sim 3 \times 10^{-39}$ C²m²/J for the photon energies of concern, and $\mu \sim 5.3 \times 10^{-30}$ Cm for Kapton. These values were determined from the limited amount of experimental data available [6, 7].

A further temperature related complication is the fact that these dielectric foils may not cool back down to room temperature during the minute or so in between shots. Because the thermal conductivity of both Kapton and quartz foils are relatively low, the dominant heat loss mechanism is radiation. Thicker foils tends to result in higher temperature buildups, as more beam heating occurs per area; this effect is somewhat counter-balanced by the typically higher thermal emissivity of thicker foils [9]. This shot-to-shot temperature buildup effect mostly concerns the thicker FXR quartz OTR foils. Currently, a simple model assuming only radiation loss and a flat current profile gives sample shot-to-shot foil temperatures illustrated in Figure 5. Typically a flat top temperature is reached relatively quickly. In addition to the OTR modeling, these shot-to-shot curves are again also used to prevent melting of the OTR foil. If required, the detailed temperature profile in Figure 4 using the more realistic current profile could be added to this flat top model to get an approximate temperature profile which accounts for shot history.

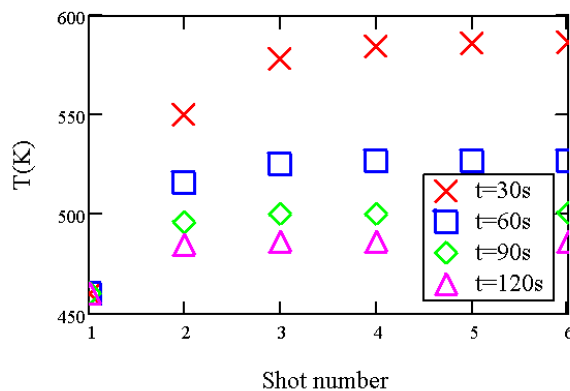


Figure 5: Post shot-to-shot temperature of a 0.38 mm thick quartz foil for uniform FXR beams of 1 cm radius assuming radiation losses only and a thermal emissivity of 0.75. Each curve represents different cooling periods in between shots.

Detector Response

Taking the results above and simulating the viewing cone of the diagnostic gives the detector response along the center vertical strip for each incident electron assuming no divergence. Figure 6 illustrates this response curve for different f-numbers. For each point along the vertical strip, the solid angle to the instrument is determined. The OTR emission from that point is then

approximated by a trapezoidal integration with limits determined by the solved solid angle. The electrons near the center emit less light due to both the anisotropic nature of OTR and the lowered permittivity from the Debye model. These response curves are then multiplied by the same input current profiles used to determine the temperature of the foil in order to produce the complete synthetic diagnostic solution.

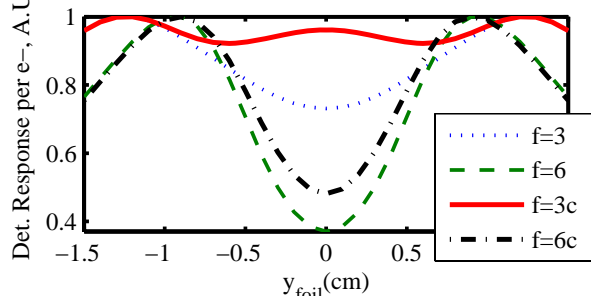


Figure 6: Detector response per incident beam electron along a Kapton center vertical strip using different f-number settings. The first two curves use the ϵ profile in Figure 4, while the last two assumes a constant $\epsilon=3.4$. The responses have been normalized for comparison.

RESULTS

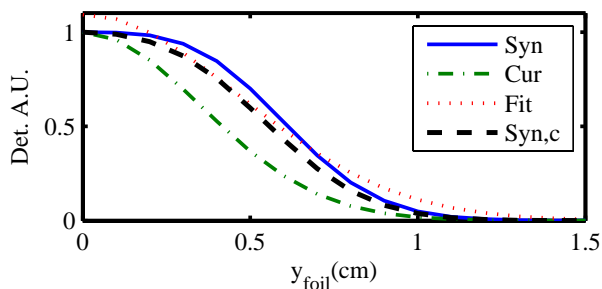


Figure 7: $f=6$ Synthetic diagnostic profiles for a Gaussian beam current profile using the response curves in Figure 6. A Gaussian fit of the first diagnostic profile gives an $r_{rms} \sim 0.66$ cm, indicating an observed r_{rms} that is $\sim 30\%$ greater than the real beam r_{rms} . The last curve shows the synthetic profile using a constant $\epsilon=3.4$. It has a fitted $r_{rms} \sim 0.62$ cm, 24% greater than the real beam r_{rms} .

Multiplying the detector responses with the Gaussian beam current profile results in the sample synthetic spot-size profiles shown in Figure 7. This simulated profile is plainly wider than the input beam current profile. As shown, this additional width is caused by both the anisotropic nature of the OTR emission and decreased emission due to the foil temperature profile. For the higher f-number cases, hollow spot-size profiles with twin peaks are predicted for beams with no divergence. The finite divergence of a real beam will eliminate some of the hollowness.

In general, the simulations predict that the observed spot-size will be larger than the real beam spot-size, especially at high f-numbers. Figure 8 plots the simulated spot size FWHM on Kapton versus the input beam current

profile FWHM. The FWHM is used simply here since Gaussian fits do not work well with hollow or flat profiles. Using these types of curves prepared with some estimate or knowledge of the real beam divergence and accurate permittivity data, the real current radii can be calculated quickly based on observed spot size radii data.

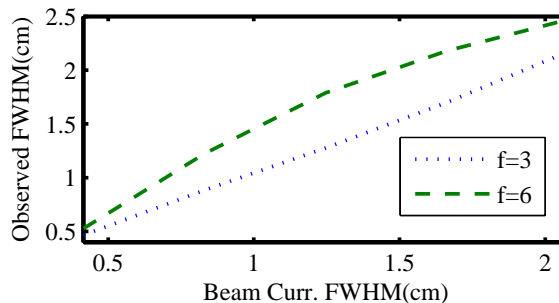


Figure 8: Observed FWHM versus Beam FWHM for Gaussian current profiles at different f-numbers. The low f-number setting gives the best FWHM match.

SUMMARY

OTR spot-size measurements of the FXR electron beam using dielectric foils were simulated with a detailed model which account for finite permittivity and temperature profiles of the foil, and the diagnostic optical setup. The simulations predict that in some scenarios the observed spot-size radius will be larger than the beam current radius due to depressed OTR emission in the spot center. These studies ultimately permit the real beam radius to be extracted from experimental spot-size data. The simulations will be improved with a refinement of the permittivity model and the incorporation of measured beam divergences. Additionally, charging of the foil is a possibility and should be studied. The successful implementation of these models would allow the routine use of dielectric foils for OTR diagnostics, and hence result in greater design flexibility and operation.

REFERENCES

- [1] B. Kulke et al., "Design of a 20 MeV, 4 kA Linear Induction Accelerator", IEEE Conf. Plasma Science, 1980.
- [2] M. Ong et al., "FXR fast beam imaging diagnostics", 12th IEEE Pulse Power Conf., 1999.
- [3] G. P. Le Sage, UCRL-ID-153254, LLNL Technical Report, 2002.
- [4] J.S. Jacob et al., UCRL-TR-214037, LLNL Technical Report, 2005.
- [5] M. L. Ter-Mikaelian, High Energy Electromagnetic Processes in Condensed Media, Wiley-Interscience, New York, 1972, Equations 25.16 and 25.18.
- [6] "Summary of Properties for Kapton Polyimide Films", DuPont Company.
- [7] E. T. Arakawa et al., J. Appl. Phys., 52, 1981.
- [8] P. Atkins, Physical Chemistry, 6th ed., W.H. Freeman and Co., New York, 1998, pg. 656.
- [9] E. J. Simburger et al., 28th IEEE Photovoltaic Specialists Conf., 1053-1056, 2000.